












The Bright γ -ray Flare of 3C 279 in 2015 June: *AGILE* Detection and Multifrequency Follow-up Observations

C. Pittori^{1,2} , F. Lucarelli^{1,2} , F. Verrecchia^{1,2} , C. M. Raiteri³ , M. Villata³, V. Vittorini⁴ , M. Tavani^{4,5,6} , S. Puccetti⁷ , M. Perri^{1,8}, I. Donnarumma^{4,7}, S. Vercellone⁹ , J. A. Acosta-Pulido^{10,11}, R. Bachev¹², E. Benítez¹³, G. A. Borman¹⁴, M. I. Carnerero³, D. Carosati^{15,16}, W. P. Chen¹⁷, Sh. A. Ehgamberdiev¹⁸, A. Goded^{10,11}, T. S. Grishina¹⁹, D. Hiriart²⁰, H. Y. Hsiao¹⁷, S. G. Jorstad^{21,22}, G. N. Kimeridze²³, E. N. Kopatskaya¹⁹, O. M. Kurtanidze^{23,24}, S. O. Kurtanidze²³, V. M. Larionov^{19,25}, L. V. Larionova¹⁹, A. P. Marscher²¹, D. O. Mirzaqulov¹⁸, D. A. Morozova¹⁹, K. Nilsson²⁶, M. R. Samal¹⁷, L. A. Sigua²³, B. Spassov¹², A. Strigachev¹², L. O. Takalo²⁷, L. A. Antonelli¹, A. Bulgarelli²⁸, P. Cattaneo²⁹, S. Colafrancesco³⁰, P. Giommi⁷, F. Longo³¹, A. Morselli³² , and F. Paoletti^{4,33}

¹ ASI Space Science Data Center (SSDC), Via del Politecnico snc, I-00133 Roma, Italy; carlotta.pittori@ssdc.asi.it

² INAF, Osservatorio Astronomico di Roma, via Frascati 33, I-00078 Monte Porzio Catone (Roma), Italy

³ INAF, Osservatorio Astrofisico di Torino, via Osservatorio 20, I-10025 Pino Torinese, Italy

⁴ INAF/IAPS–Roma, Via del Fosso del Cavaliere 100, I-00133 Roma, Italy

⁵ Univ. “Tor Vergata”, Via della Ricerca Scientifica 1, I-00133 Roma, Italy

⁶ Gran Sasso Science Institute, viale Francesco Crispi 7, I-67100 L’Aquila, Italy

⁷ Agenzia Spaziale Italiana (ASI), Via del Politecnico snc, I-00133 Roma, Italy

⁸ INAF–OAR, via Frascati 33, I-00078 Monte Porzio Catone (Roma), Italy

⁹ INAF, Osservatorio Astronomico di Brera, Via E. Bianchi 46, I-23807 Merate (LC), Italy

¹⁰ Instituto de Astrofísica de Canarias (IAC), E-38205 La Laguna, Tenerife, Spain

¹¹ Departamento de Astrofísica, Universidad de La Laguna, E-38206 La Laguna, Tenerife, Spain

¹² Institute of Astronomy and National Astronomical Observatory, Bulgarian Academy of Sciences,

72 Tsarigradsko shosse Boulevard, 1784 Sofia, Bulgaria

¹³ Instituto de Astronomía, Universidad Nacional Autónoma de México, Apdo. Postal 70-264, 04510 Cd. de México, Mexico

¹⁴ Crimean Astrophysical Observatory, P/O Nauchny, 298409, Russia

¹⁵ EPT Observatories, Tjarafe, E-38780 La Palma, Spain

¹⁶ INAF, TNG Fundación Galileo Galilei, E-38712 La Palma, Spain

¹⁷ Graduate Institute of Astronomy, National Central University, Jhongli City, Taoyuan County 32001, Taiwan

¹⁸ Ulugh Beg Astronomical Institute, Maidanak Observatory, 33 Astronomicheskaya str., Tashkent, 100052, Uzbekistan

¹⁹ Astronomical Institute, St. Petersburg State University, 198504 St. Petersburg, Russia

²⁰ Instituto de Astronomía, Universidad Nacional Autónoma de México, Ensenada, Baja California, Mexico

²¹ Institute for Astrophysical Research, Boston University, 725 Commonwealth Avenue, Boston, MA 02215, USA

²² Astronomical Institute, St. Petersburg State University, Universitetskij Pr. 28, Petrodvorets, 198504 St. Petersburg, Russia

²³ Abastumani Observatory, Mt. Kanobili, 0301 Abastumani, Georgia

²⁴ Engelhardt Astronomical Observatory, Kazan Federal University, Tatarstan, Russia

²⁵ Pulkovo Observatory, 196140 St. Petersburg, Russia

²⁶ Finnish Centre for Astronomy with ESO (FINCA), University of Turku, Väisäläntie 20, FI-21500 Piikkiö, Finland

²⁷ Tuorla Observatory, Department of Physics and Astronomy, University of Turku, FI-20014 Turku, Finland

²⁸ INAF-IASF Bologna, via Gobetti 101, I-40129 Bologna, Italy

²⁹ INFN-Pavia, via Bassi 6, I-27100 Pavia, Italy

³⁰ School of Physics, University of the Witwatersrand, Johannesburg Wits 2050, South Africa

³¹ Dipartimento di Fisica, Univ. di Trieste and INFN, via Valerio 2, I-34127 Trieste, Italy

³² INFN Roma “Tor Vergata”, via della Ricerca Scientifica 1, I-00133 Roma, Italy

³³ East Windsor RSD, 25a Leshin Lane, Hightstown, NJ 08520, USA

Received 2018 January 17; revised 2018 February 19; accepted 2018 February 20; published 2018 March 28

Abstract

We report the *AGILE* detection and the results of the multifrequency follow-up observations of a bright γ -ray flare of the blazar 3C 279 in 2015 June. We use *AGILE* and Fermi gamma-ray data, together with Swift X-ray and optical-ultraviolet data, and ground-based GASP-WEBT optical observations, including polarization information, to study the source variability and the overall spectral energy distribution during the γ -ray flare. The γ -ray flaring data, compared with as yet unpublished simultaneous optical data that will allow constraints on the big blue bump rising disk luminosity, show very high Compton dominance values of ~ 100 , with the ratio of γ -ray to optical emission rising by a factor of three in a few hours. The multiwavelength behavior of the source during the flare challenges one-zone leptonic theoretical models. The new observations during the 2015 June flare are also compared with already published data and nonsimultaneous historical 3C 279 archival data.

Key words: galaxies: active – gamma rays: galaxies – polarization – quasars: individual (3C 279) – radiation mechanisms: non-thermal – X-rays: general

1. Introduction

Blazars are a subclass of radio-loud active galactic nuclei with relativistic jets pointing toward the observer (Urry & Padovani 1995). Their emission extends from the radio band to the γ -ray band above 100 MeV up to TeV γ -rays, and it is

dominated by variable nonthermal processes. They come in two main flavors, with very different optical spectra: Flat Spectrum Radio Quasars (FSRQs) that have strong, broad optical emission lines; and BL Lacertae objects (BL Lacs) with an optical spectrum that can be completely featureless or can

show, at most, weak emission lines and some absorption features (e.g., see Giommi et al. 2012 for a detailed review on blazar classification). The blazar spectral energy distribution (SED) is, in general, characterized by two broad bumps: the low-energy one, spanning from the radio to the X-ray band, is attributed to synchrotron radiation, while the high-energy one, from the X-ray to the γ -ray band, is thought to be due to inverse Compton (IC) emission. In the leptonic scenario, this second component is due to relativistic energetic electrons scattering their own synchrotron photons—Synchrotron self-Compton (SSC)—or photons external to the jet—External Compton (EC). Blazars of both flavors have been found to be highly variable and particularly so in γ -rays.³⁴ The correlated variability between X-rays and γ -rays is usually well explained in the SSC or EC framework (Ghisellini et al. 1998). In fact, a new class of “orphan” γ -ray flares from FSRQ blazars is now emerging from observations, challenging the current simple one-zone leptonic models. In particular, a number of γ -ray flares from some extensively monitored FSRQs, such as 3C 279, do not correlate with optical and soft X-ray events of comparable power and timescales; see, for example, the results of a previous multiwavelength campaign on 3C 279 during flaring states in 2013–2014 (Hayashida et al. 2015).

Gamma-ray observations of flaring blazars and simultaneous multiwavelength data are thus the key to investigate possible alternative theoretical scenarios, such as a recently proposed model based on a mirror-driven process within a clumpy jet inducing localized and transient enhancements of synchrotron photon density beyond the broad-line region (BLR; Tavani et al. 2015; Vittorini et al. 2017). Other scenarios consider special structures, such as spine-sheath jet layers radiative interplay (Tavecchio & Ghisellini 2008; Sikora et al. 2016) or “rings” of fire, i.e., synchrotron-emitting rings of electrons representing a shocked portion of the jet sheath (MacDonald et al. 2015).

3C 279 is associated with a luminous FSRQ at $z = 0.536$ (Lynds et al. 1965), with prominent broad emission lines detected in all accessible spectral bands and revealing highly variable emission. It consistently shows strong γ -ray emission, which are already clearly detected by EGRET (Hartman et al. 1992; Kniffen et al. 1993), *AGILE* (Giuliani et al. 2009), *Fermi*-Hayashida et al. 2012, 2015), and also detected above 100 GeV by MAGIC (Albert et al. 2008). The central black hole mass estimates are in the range of $(3\text{--}8) \times 10^8 M_{\odot}$ (Gu et al. 2001; Woo & Urry 2002; Nilsson et al. 2009). The 3C 279 jet features strings of compact plasmoids, as indicated by radio observations (Hovatta et al. 2009), which may be a by-product of the magnetic reconnection process (Petropoulou et al. 2016), even though it must be taken into account that the superluminal knots observed in Very Long Baseline Interferometry images are probably much larger structures than the reconnection plasmoids formed on kinetic plasma scales, hence this connection is uncertain (Chatterjee et al. 2008).

Here we present the results of a multiband observing campaign on the blazar 3C 279 triggered by the detection of intense γ -ray emission above 100 MeV by the *AGILE* satellite in 2015 June (Lucarelli et al. 2015). The source is one of the γ -ray blazars monitored by the *GLAST-AGILE*³⁵ Support Program (GASP) of the Whole Earth Blazar Telescope

(WEBT) Collaboration³⁶ (Bottcher et al. 2007; Larionov et al. 2008; Villata et al. 2008; Abdo et al. 2010).

The *AGILE*-Gamma-ray Imaging Detector (–GRID) γ -ray data of 3C 279 in 2015 June are compared with as yet unpublished (*R*-band) optical GASP-WEBT observations during the flare, including the percentage and angle of polarization, and with *Fermi*-Fermi-Large Area Telescope (–LAT; Paliya et al. 2015; Ackermann et al. 2016) and other multiwavelength data from the *Swift*-Ultraviolet/Optical Telescope (–UVOT) and the *Swift*-X-Ray Telescope (–XRT) Target of Opportunities (ToO). The analysis of the source multiwavelength behavior is crucial in order to study the correlation (if any) of the γ -ray radiation with the optical-ultraviolet (–UV) and X-ray emissions. The 2015 June flaring data are also compared with nonsimultaneous archival data from the NASA/IPAC Extragalactic Database and from the ASI Space Science Data Center (SSDC, previously known as ASDC).

2. Observations and Data Analysis

2.1. *AGILE* Observations

AGILE (Tavani et al. 2009) is a small mission of the Italian Space Agency (ASI) devoted to γ -ray astrophysics, operating in a low Earth orbit since 2007 April 23. The main *AGILE* instrument is GRID, which is sensitive in the energy range 30–50 GeV. *AGILE*-GRID consists of a silicon-tungsten tracker, a cesium iodide mini-calorimeter, and an anticoincidence system (AC) made of segmented plastic scintillators.

The *AGILE* Quick Look (QL) alert system (Pittori 2013; Bulgarelli et al. 2014) detected increased γ -ray emission from 3C 279 starting from 2015 June 13 (MJD = 57186) and lasted up to 2015 June 17 (MJD = 57190).

The *AGILE*-GRID data were analyzed using the *AGILE* Standard Analysis Pipeline (see Vercellone et al. 2008 for a description of the *AGILE* data reduction). Counts, the exposure, and Galactic diffuse background maps for energy $E \geq 100$ MeV were created, including all events collected up to 60° off-axis. Scientific data acquisition is inhibited during the South Atlantic Anomaly passages, and we rejected all γ -ray events whose reconstructed directions form angles with the satellite–Earth vector $\leq 80^\circ$ to reduce the γ -ray Earth albedo contamination. We used the latest public *AGILE* software Package (*AGILE* SW 5.0 SourceCode) with calibration files (I0023), and the *AGILE* γ -ray diffuse emission model (Giuliani et al. 2004), which is publicly available at the SSDC site.³⁷

2.2. GASP-WEBT Observations

Optical observations of 3C 279 were carried out by the GASP-WEBT Collaboration in the Cousins’ *R* band. Data were provided by the following observatories: Abastumani (Georgia), Belogradchik (Bulgaria), Crimean (Russia), Lowell (USA; Perkins telescope), Lulin (Taiwan), Mt. Maidanak (Uzbekistan), Roque de los Muchachos (Spain; KVA), San Pedro Martir (Mexico), Skinakas (Greece), St. Petersburg (Russia), Teide (Spain; IAC80 and STELLA-I), and Tjarafe (Spain). The calibrated source magnitude was obtained by differential photometry with respect to Stars 1, 2, 3, and 5 of the photometric sequence by Raiteri et al. (1998). The optical light curve (see Section 3.1) was visually inspected and checked. No significant offset was noticed between different data sets.

³⁴ The SED movie of the blazar 3C 279 from 2008.05 to 2016.37 by P. Giommi: <http://www.youtube.com/watch?v=o0JJBakFUXQ>.

³⁵ GLAST refers to the Fermi Gamma-ray Space Telescope, formerly known as the Gamma-ray Large Area Space Telescope.

³⁶ <http://www.oato.inaf.it/blazars/webt/>

³⁷ <http://agile.ssdsc.asi.it/publicsoftware.html>

Table 1
Swift Follow-up Observations of 3C 279 Following the *AGILE* γ -ray Flare Alert in 2015 June, and On-source Net Exposures in the Pointing Observing Mode for the XRT (Photon Counting Readout Mode) and UVOT Instruments within Each Observation

OBS Start Time (UTC)	MJD	XRT Exposure (s)	UVOT Exposure (s)	obsID
2015 Jun 15 14:27:58	57188.6028	1987.8	1994.1	00035019176
2015 Jun 16 03:27:59	57189.1444	958.9	961.7	00035019180
2015 Jun 16 16:04:58	57189.6701	934.0	936.1	00035019181
2015 Jun 17 04:40:59	57190.1951	936.5	938.2	00035019185
2015 Jun 17 20:59:58	57190.8750	489.5	488.6	00035019187
2015 Jun 18 04:37:59	57191.1930	1246.1	1249.2	00035019188

Polarimetric information in the *R* band was acquired at the Crimean, Lowell, San Pedro Martir, and St. Petersburg observatories.

2.3. *Swift* ToO Observations

Following the 3C 279 γ -ray flare detected by *AGILE*, a prompt *Swift* target of opportunity observation was performed on 2015 June 15, for a total net exposure time of about 2.0 ks. Another five *Swift*-XRT observations were carried out on 2015 June 16–18. A summary of these observations is given in Table 1, where the net exposures with the XRT and UVOT instruments are also reported.

2.3.1. XRT Observations

The XRT onboard *Swift* (Gehrels et al. 2004) is sensitive to the 0.3–10 keV X-ray energy band (Burrows et al. 2004). The six 2015 June XRT follow-up observations of 3C 279 were all carried out using the most sensitive Photon Counting readout mode for a total net exposure time of about 6.5 ks. The XRT data sets were first processed with the XRTDAS software package (v.3.1.0) developed at SSC and distributed by the High Energy Astrophysics Science Archive Research Center (HEASARC) within the HEASoft package (v. 6.17). Event files were calibrated and cleaned with standard filtering criteria with the *xrtpipeline* task using the calibration files available in the version 20150721 of the *Swift*-XRT calibration database (CALDB). Except for the last two observations, the source count rate was initially high enough to cause some photon pile-up in the inner 3 pixels radius circle centered on the source position, as derived from the comparison of the observed point-spread function (PSF) profile with the analytical model derived in Moretti et al. (2005). We avoided pile-up effects by selecting events within an annular region with an inner radius of 3 pixels and an outer radius of 30 pixels. The background was extracted from a nearby source-free annular region of the 50/90 pixel inner/outer radius. The ancillary response files were generated with the *xrtmkarf* task, applying corrections for the PSF losses and CCD defects using the cumulative exposure map. The response matrices available in the *Swift* CALDB at the time of analysis were used. The source spectra were binned to ensure a minimum of 30 counts per bin.

For all *Swift* ToO observations, fits of the XRT spectra were performed using the XSPEC package. The observed X-ray spectrum (0.3–10 keV) can be fit by an absorbed power-law model with a HI column density that is consistent with the Galactic value in the direction of the source, $n_{\text{H}} = 2.2 \times 10^{20} \text{ cm}^{-2}$ (Kalberla et al. 2005). The results of photon index

Table 2

Results of the X-ray Spectral Analysis of the *Swift*-XRT Follow-up Data

XRT Date Start (UTC)	Photon Index	XRT Flux (0.3–10 keV) ($\text{erg cm}^{-2} \text{ s}^{-1}$)
2015 Jun 15 14:32	1.36 ± 0.06	$(5.5 \pm 0.4) \times 10^{-11}$
2015 Jun 16 03:31	1.32 ± 0.08	$(9.4 \pm 0.8) \times 10^{-11}$
2015 Jun 16 16:08	1.4 ± 0.1	$(3.5 \pm 0.5) \times 10^{-11}$
2015 Jun 17 04:44	1.4 ± 0.1	$(2.7 \pm 0.4) \times 10^{-11}$
2015 Jun 17 21:02	1.3 ± 0.2	$(2.0 \pm 0.5) \times 10^{-11}$
2015 Jun 18 04:41	1.5 ± 0.1	$(1.7 \pm 0.2) \times 10^{-11}$

Note. The errors are at 90% level of confidence, and fluxes are corrected for the galactic absorption

Table 3

Results of the Analysis of the *Swift*-UVOT ToO Follow-up Data

UVOT Date Start (UTC)	Filter (of the day)	UVOT Magnitude
2015 Jun 15 14:33	U	14.93 ± 0.03
2015 Jun 16 03:32	W2	15.35 ± 0.04
2015 Jun 16 16:09	W2	15.44 ± 0.04
2015 Jun 17 04:45	M2	15.38 ± 0.04
2015 Jun 17 21:04	M2	15.64 ± 0.05
2015 Jun 18 04:41	W1	15.65 ± 0.04

Note. Observed magnitudes, which are not corrected for galactic extinction, and errors at the 1σ confidence level.

and fluxes corrected for the Galactic absorption for each follow-up observation are shown in Table 2.

2.3.2. UVOT Observations

Co-aligned with the XRT, the *Swift*-UVOT instrument (Roming et al. 2005) provides simultaneous UV and optical coverage (170–650 nm). UVOT ToO observations were performed with the optical/UV filter of the day, namely U, W2, and M2, as described in Table 3. We performed aperture photometry using the standard UVOT software distributed within the HEASoft package (v. 6.17), and the calibration included in the latest release of the CALDB. The values of the UVOT observed magnitudes of the source are given in Table 3. Source counts were extracted from an aperture of the 5 arcsec radius for all filters, while the background ones were extracted from an annular region of the inner aperture 26 arcsec and size 9 arcsec, then the source counts were converted to fluxes using the standard zero points (Breeveld et al. 2011). The fluxes were

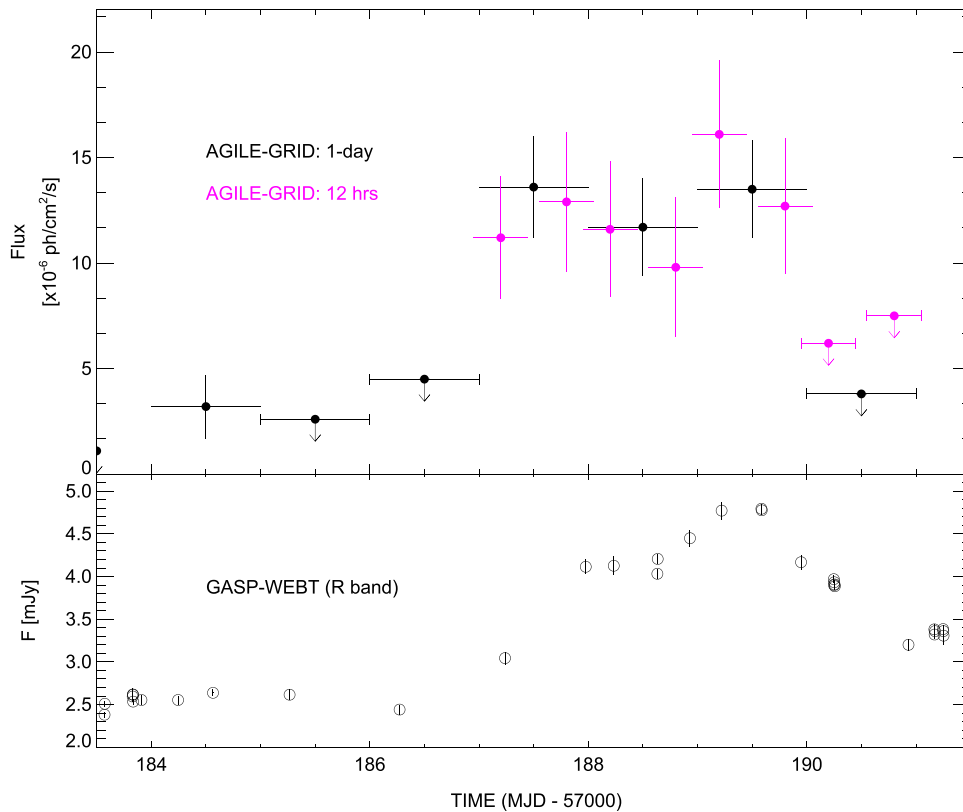


Figure 1. Top panel: *AGILE*-GRID 3C 279 γ -ray light curve ($E \geq 100$ MeV) during the 2015 June flare. Bottom panel: simultaneous GASP-WEBT optical data (R-band, de-absorbed flux densities), showing a well-defined maximum peaking around MJD = 57189.

finally dereddened using the appropriate value $E(B-V) = 0.0245$, taken from Schlegel et al. (1998) and Schlafly & Finkbeiner (2011), with $A_{\lambda}/E(B-V)$ ratios calculated for UVOT filters using the mean Galactic interstellar extinction curve from Fitzpatrick (1999). These fluxes were then included in the multiwavelength SED (see Section 3.2).

2.4. Fermi-LAT Observations

We compared *AGILE* γ -ray observations with published *Fermi*-LAT data from Ackermann et al. (2016), and with public *Fermi* data obtained from the online data analysis tool at SSCC.³⁸ As described in Ackermann et al. (2016), events in the energy range 100 MeV–300 GeV were extracted within a 15° acceptance cone of the Region of Interest (ROI) centered on the location of the source. Gamma-ray fluxes and spectra were determined by an unbinned maximum likelihood fit with `gtlike`. The background model included all known γ -ray sources within the ROI from the third *Fermi*-LAT catalog (Acero et al. 2015). Additionally, the model included the isotropic and Galactic diffuse emission components. Flux normalization for the diffuse and background sources were left free in the fitting procedure.

3. RESULTS

3.1. Light Curves

In Figure 1, we present the simultaneous (and as yet unpublished) *AGILE* γ -ray and GASP-WEBT optical light

curves during the 3C 279 flare in 2015 June. In order to produce the *AGILE* light curve, we divided the data collected in the period from 2015 June 11 to 18 (MJD: 57184–57191) in 24 and 12 hr timebins. To derive the estimated flux of the source, we ran the *AGILE* Multi-Source Maximum Likelihood Analysis (ALIKE) task with an analysis radius of 10° . The ALIKE was carried out by fixing the position of the source to its nominal radio position (Johnston et al. 1995), $(l, b) = (305.104, 57.062)$ (deg) and using Galactic and isotropic diffuse emission parameters (GAL-ISO) fixed at the values estimated during the two weeks preceding the analyzed *AGILE* data set.

The extended GASP-WEBT optical light curve (R-band magnitude) of 3C 279 since the end of 2014, including the γ -ray flaring period (MJD: 57010–57220), is shown in Figure 2. It includes the polarization percentage P and electric vector polarization angle (EVPA) variations. The total brightness variation in this period is ~ 1.5 magnitude, from $R = 16.07$ at MJD = 57142.1 to $R = 14.58$ at MJD = 57189.6.

The multiwavelength behavior of the source during the flare is then summarized in Figure 3, which includes γ -ray light curves, as observed by *AGILE*-GRID and *Fermi*-LAT, the prompt *Swift*-XRT X-ray followup, and the simultaneous GASP-WEBT de-absorbed optical flux densities and polarimetric data.

A well-defined maximum peaking around MJD = 57189 is visible at γ -rays, which is in agreement with the optical observations. The degree of observed polarization P remains always high, ranging between about 9% and 30%. The maximum observed value occurs at MJD = 57190.2, and the daily sampling allows to identify a 1 day delay of the P

³⁸ <https://tools.asdc.asi.it/?&searchtype=fermi>

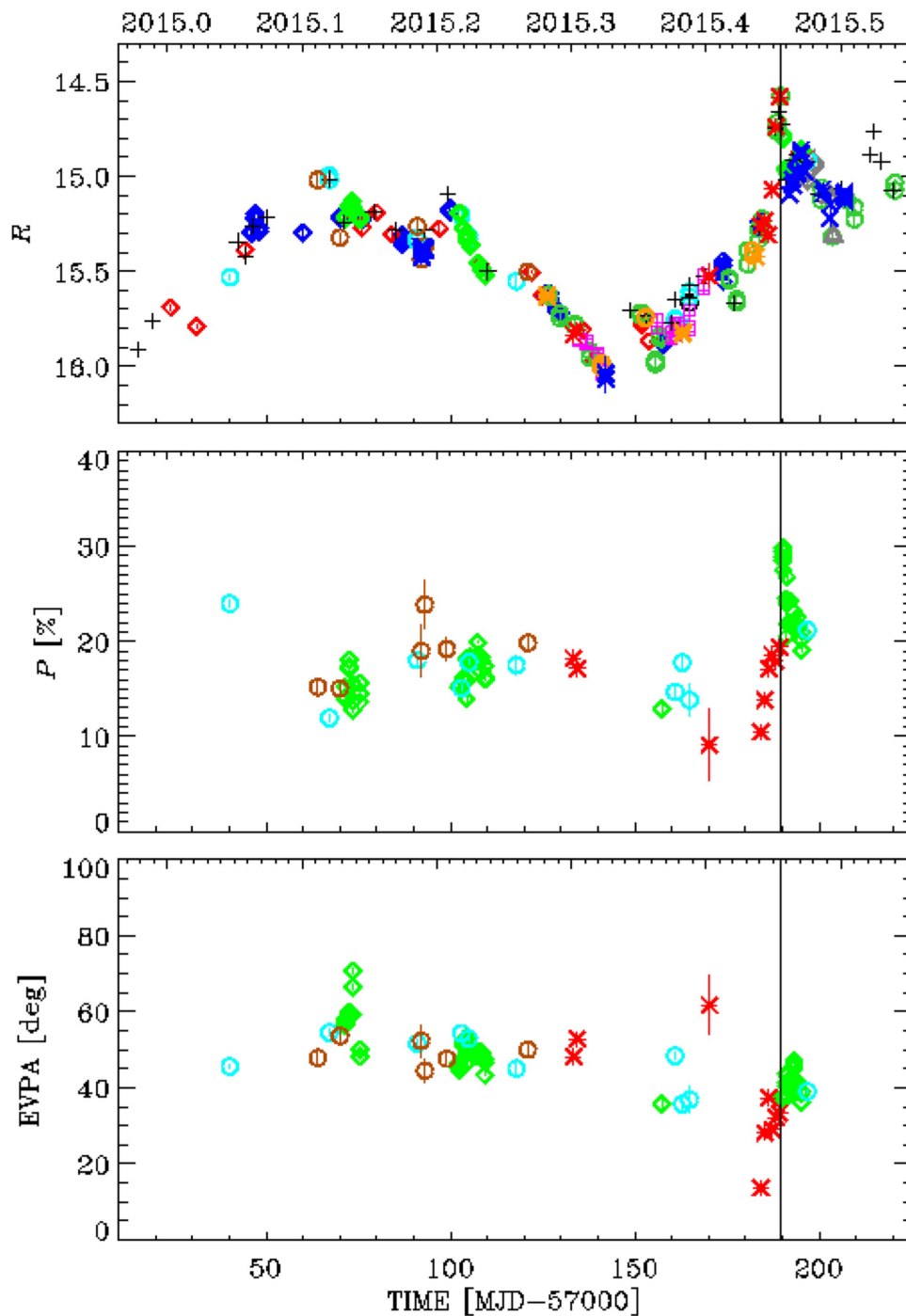


Figure 2. Photometric and polarimetric optical data in the R band acquired by the GASP-WEBT Collaboration from 2014 December 9 (MJD = 57000) to 2015 July 17 (MJD = 57220). The corresponding time in calendar years is shown above the figure. Different colors and symbols highlight data points from different telescopes (see the text for the full list). The vertical line indicates the optical flux measured maximum (MJD = 57189.585).

maximum after the flux peak observed at optical and γ -ray frequencies. The rise and the following decrease of P and flux is accompanied by a rotation of the electric vector polarization angle of about 30° in 10 days.

As shown in Figure 3's third panel, the X-ray flux variability also appears correlated with the γ -ray and optical ones. The peak X-ray flux value occurs at MJD = 57189.14, and it is about a factor of about four higher than the one observed one day later (see Table 2).

3.2. Spectral Energy Distribution

Figure 4 shows the 3C 279 broadband SED obtained with the help of the SSDC SED Builder tool.³⁹ Simultaneous *AGILE*, GASP-WEBT, *Swift*-XRT, and *Swift*-UVOT data during the 2015 June flare are shown in red. Average γ -ray flux excluding the flaring period and other public non-simultaneous archival data in other wavelengths are shown in gray.

³⁹ <http://tools.asdc.asi.it/SED>

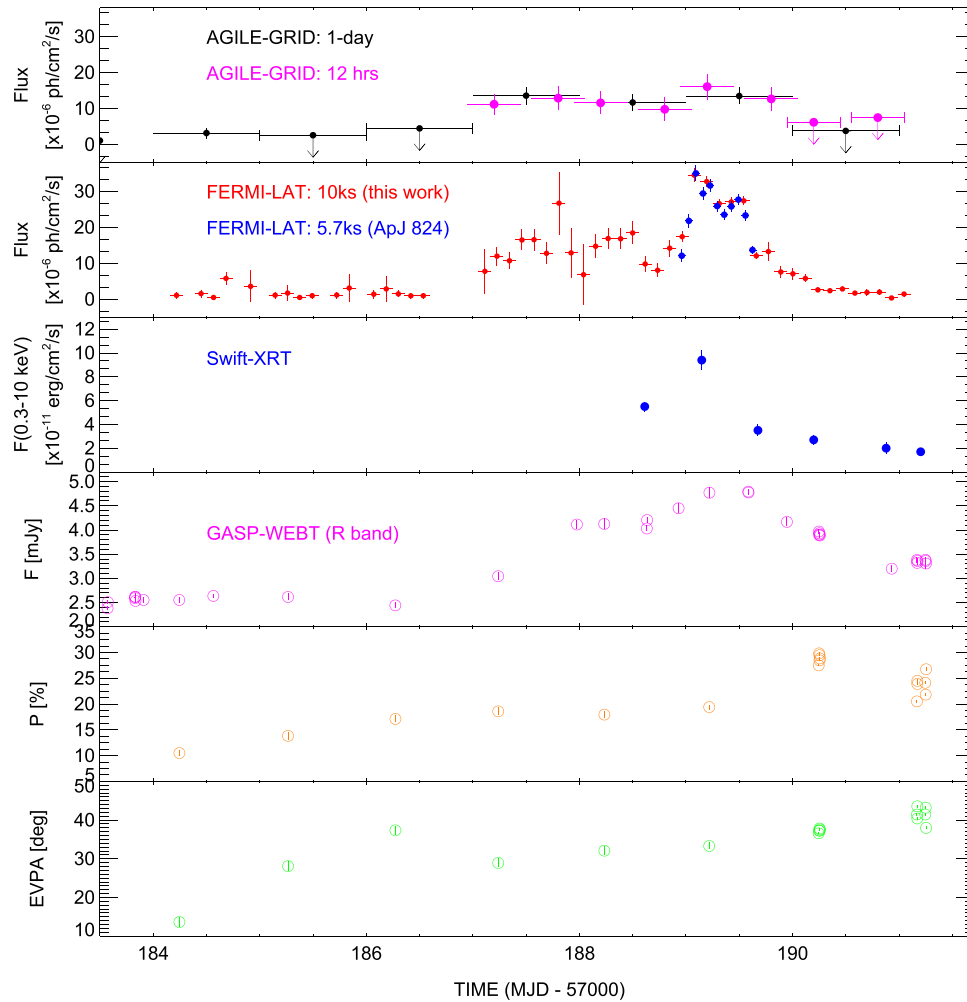


Figure 3. Multiwavelength light curves of 3C 279 in 2015 June: γ -rays ($E \geq 100$ MeV), as observed by *AGILE*-GRID and *Fermi*-LAT, the prompt *Swift*-XRT X-ray followup, and simultaneous GASP-WEBT photometric and polarimetric optical data. Second panel: *Fermi*-LAT blue points are from Ackermann et al. (2016), and the red points are from the public online *Fermi* data analysis tool at SSDC. In the last three panels, we report a selection of the full data set of GASP-WEBT observations already presented in Figure 2, zoomed in around the γ -ray peak.

We have performed the *AGILE* spectral analysis of the peak γ -ray activity, corresponding to the period between 2015 June 14 (MJD = 57187.0) and 2015 June 17 (MJD = 57190.0) over three energy bins: 100–200, 200–400, and 400–1000 MeV. A simple power-law spectral fitting gives a photon index of $\Gamma_\gamma = (2.14 \pm 0.11)$, which is consistent within the errors with the values reported by *Fermi* (Paliya et al. 2015; Ackermann et al. 2016). Moreover, we estimated the average γ -ray fluxes obtained by integrating in the whole *AGILE* energy band (100 MeV–50 GeV) during three time periods, defined as a *pre-outburst* (MJD: 57184–57187), a *flare* (MJD: 57187–57190), and a *post-flare* (MJD: 57190–57193). The corresponding *AGILE* integral γ -ray fluxes and spectral indices are summarized in Table 4. Historically, this is the largest γ -ray flare (≥ 100 MeV) of 3C 279 ever observed, including recent activity reported in Bulgarelli et al. (2017).

The SED during the flare (red points in Figure 4) indicates a very high “Compton dominance”: the ratio of the IC peak to the synchrotron 1 is of the order of 100. Specifically, the γ -ray spectrum integrated over 1 day timebins rises by a factor of ~ 3 in a few hours (as shown in Figure 3), yielding a Compton dominance of about 100, and attaining values up to ~ 200 when integrating on even shorter timescales (Ackermann et al. 2016).

4. Simple Flare Modeling and Discussion

In this section, we estimate the parameters of a tentative simple modeling of the multiwavelength 3C 279 data acquired during the 2015 flare. The model parameter values obtained here can be used as reference input for a more detailed further theoretical analysis.

In the framework of the one-zone leptonic model for FSRQs (see e.g., Paggi et al. 2011), the optical and UV data acquired during the 2015 June flare, presented here, would constrain the luminosity of the accretion disk to $L_D \leq 10^{46}$ erg s $^{-1}$. We note that this value is larger, by a factor of about 3, than the disk luminosity previously inferred for 3C 279 (Raiteri et al. 2014).

Taking into account also the simultaneous soft X-ray data and the observed variability, we can determine empirical constraints on the model parameters: the size l , the bulk boost factor Γ , the energetic content in magnetic field B , and the electron energy distribution $n_e(\gamma)$ of the emitting region. We assume that the relativistic electrons have a double power-law energy-density distribution:

$$n_e(\gamma) = \frac{K \gamma_b^{-1}}{(\gamma/\gamma_b)^{\zeta_1} + (\gamma/\gamma_b)^{\zeta_2}} [\text{cm}^{-3}], \quad (1)$$

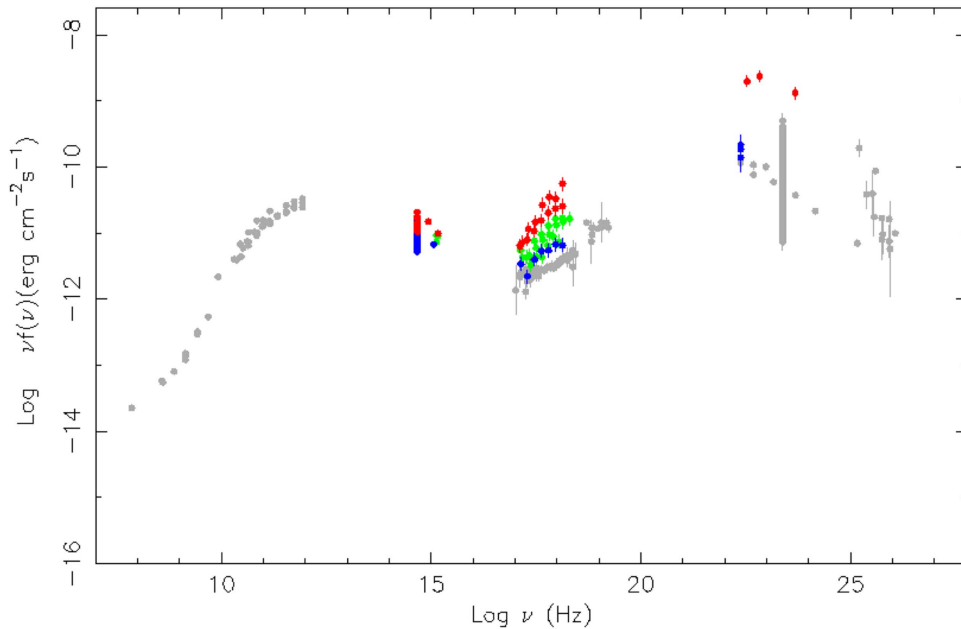


Figure 4. 3C 279 broadband SED obtained with the help of the SSDC SED Builder tool (v. 3.2). Red points: *AGILE* data during the 2015 June γ -ray flare (around MJD: 57187–57190), and simultaneous *GASP-WEBT*, *Swift-UVOT*, and *Swift-XRT* ToO data. Green points: *Swift-UVOT* and *Swift-XRT* follow-up data covering approximately 48 hr after the γ -ray peak emission (see Table 1). Blue points: post-flare 2015 data from *GASP-WEBT* (up to MJD = 57220), *Swift-UVOT*, *Swift-XRT* (MJD = 57191), and *AGILE* data (weekly averaged flux above 100 MeV from MJD = 57197.5 to 57218.5). Gray points: public nonsimultaneous archival data from SSDC (CRATES, DIXON, NVSS, PKSCAT90, PMN, VLSS, AT20GCAT, PLANCK, WMAP5, *Swift-BAT*, IBIS/ISGRI, *BeppoSAX*, *AGILE-GRID*, *Fermi-LAT*, and MAGIC).

Table 4
AGILE γ -ray Fluxes and Spectral Indices

Label	T_{start} MJD	T_{stop} MJD	$F(E \geq 100 \text{ MeV})$ ($10^{-6} \text{ ph cm}^{-2} \text{ s}^{-1}$)	Γ_{γ}
Pre-outburst	57184.0	57187.0	(1.7 ± 0.7)	(2.0 ± 0.4)
Flare	57187.0	57190.0	(13.0 ± 1.3)	(2.1 ± 0.1)
Post-flare	57190.0	57193.0	(1.0 ± 0.5)	...

Note. Over the considered 3 day time periods, the source flux increases of factor of about 7, then rapidly drops more than a factor of 10 in the post-flare, with insufficient statistics for the spectral analysis.

where K is a normalization factor, γ_b is the break Lorentz factor, ζ_1 and ζ_2 are the double power-law spectral indices below and above the break, respectively.

These electrons interact via the IC process with the synchrotron photons internal to the same emitting region, with the external photons coming from the accretion disk and from the BLR. From distances $R_{\text{BLR}} \simeq 0.1 \text{ pc}$, the latter reflects a fraction $\xi \simeq \text{few } \%$ of the disk radiation. In Figure 5, we show our one-zone SED model of the 2015 June flare of 3C 279 for γ -ray fluxes averaged on 1 day timescales. If we assume the emitting region located at a distance $R < R_{\text{BLR}}$ from the central black hole, then seed photons coming from BLR are good candidates to be scattered into γ -rays of observed energies $\geq 100 \text{ MeV}$ (see the red line in Figure 5). As shown by the blue lines in the same figure, disk photons entering the emitting region from behind are scattered mainly in the hard X-ray observed band. Instead, the internal scattering of the synchrotron photons are seen mainly in the soft X-ray band, as shown by the green lines.

In this model, we consider the emitting region placed at a distance $R = 6 \times 10^{16} \text{ cm}$ from the central black hole, while the accretion disk radiates the power $L_D = 10^{46} \text{ erg s}^{-1}$; a

fraction $\xi = 2\%$ of this is reflected back from the BLR placed at distance $R_{\text{BLR}} = 0.15 \text{ pc}$. A summary of the best-fit flare model parameters is shown in Table 5.

When the IC scattering occurs in the Thomson regime, the Compton dominance reads $q = U'_{\text{ext}}/U'_B$, i.e., the ratio of the comoving energy density of BLR seed photons $U'_{\text{ext}} \simeq (1 + \beta_{\Gamma}^2)\Gamma^2\xi L_D / (4\pi c R_{\text{BLR}}^2)$ to the energy density of the magnetic field $U'_B = B'^2/8\pi$, thus:

$$q \lesssim 0.2 \Gamma^2 \frac{(\xi/0.02)L_{D,46}}{(B'/\text{G})^2(R_{\text{BLR}}/0.1\text{pc})^2}. \quad (2)$$

For assumed disk luminosities $L_D \leq 10^{46} \text{ erg s}^{-1}$, this yields a value of $q \leq 80$. Moreover, the one-zone assumption has two other main consequences.

1. First, a strict correlation of optical and γ -ray fluxes: their variations must be of the same entity, so the Compton dominance should not vary.
2. Second, to increase the upper limit for q up to values above 100, as observed, we should consider faint magnetic fields values $B \lesssim 0.1 \text{ G}$, which would in turn imply modest electron accelerations (Mignone et al. 2013). Alternatively, we could assume bulk factors $\Gamma > 30$ (Ackermann et al. 2016), which considerably exceeds the value $\Gamma \simeq 20$ inferred from radio observations for this source (Hovatta et al. 2009), that would imply a conspicuous kinetic load in the jet.

Noticeably, the multiwavelength light curves of the flare in Figure 3 show instead that the Compton dominance rises by a factor of three or more in a half day, attaining values up to $q > 200$ in few minutes when considering the very fast and strong γ -ray variations reported in Ackermann et al. (2016). While the simple one-zone model presented here could account for the SED flaring data integrated on 1 day timescales

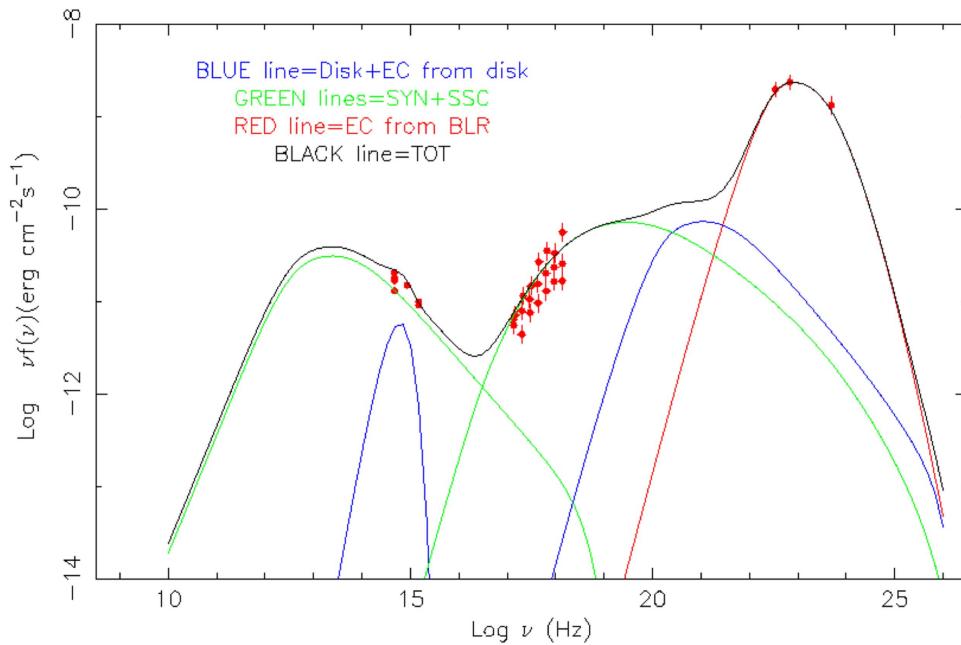


Figure 5. 3C 279: simple one-zone modeling of the 2015 June flare.

Table 5
One-zone Model Parameters for the 2015 Flare of 3C 279,
as Defined in Section 4

l (cm)	K (cm^{-3})	γ_b	γ_{\min}	ζ_1	ζ_2	Γ	B (G)
10^{16}	1100	700	180	2	4.2	20	1

(provided you assume of a very bright underlying disk), it is anyway seriously challenged by the observed strong and fast variation of the Compton dominance.

Furthermore, we notice that a single photon of energy $E = 52$ GeV was detected on MJD = 57189.62 (Paliya et al. 2015) in correspondence with the peak of optical emission and is consistent with the observed polarization fraction reaching its maximum. The modeling of this specific episode of high-energy emission goes beyond the scope of this paper and provides an additional argument for alternative modes of γ -ray emission.

5. Conclusions

In this paper, we present multifrequency optical and X-ray data simultaneous with the 2015 γ flaring activity of 3C 279. We use *AGILE-GRID* and *Fermi-LAT* (Paliya et al. 2015; Ackermann et al. 2016) γ -ray data together with the *Swift-UVOT*, the *Swift-XRT*, and as yet unpublished optical GASP-WEBT observations of 3C 279 in 2015 June. We find that from the multiwavelength light curve shown in Figure 3, the high-energy flare is partially correlated with the behavior in other energy bands. Specifically, the γ -ray flux rising by a factor $\simeq 4$ in half a day shows an optical counterpart rising only by a factor 2 or less on similar timescales. The γ -ray flux during this flare exceeds the largest 3C 279 flares previously detected, although Hayashida et al. (2015) reported an even more extreme multifrequency behavior for this source in the past; e.g., in 2013 December, the γ -ray flux above 100 MeV jumped by a factor $\simeq 5$ in a few hours without optical or X-ray

counterparts, and the Compton dominance attained values of about 300. Ackermann et al. (2016) discuss the variability of the 2015 γ -ray flare with minute timescales.

The observed spectral characteristics and the strong and fast variations of the Compton dominance challenge one-zone models, unless we assume significant variations in the field of seed photons to be IC scattered into γ -rays. We discuss in this paper a one-zone model and provide the model parameters that can be used as a theoretical model of reference. Models alternative to the standard SSC and EC might be considered (e.g., Ackermann et al. 2016). In the moving mirror model (Tavani et al. 2015; Vittorini et al. 2017) localized enhancements of synchrotron photon density may explain the occurrence of gamma-ray flares with faint or no counterpart in other bands. These localized enhancements would persist only for short periods of time, and this would explain the fact that the majority of FSRQ γ -ray flares are not orphan in nature.

We noticed that, as shown in Figure 3, the degree of observed optical polarization P appears to correlate with the optical flux F during the flare, with P peaking about one day after F . Moreover, the polarization angle rotates by at least 30° in the period encompassing the flare. However, the behavior of the polarization degree of the jet may be very different from the observed one, due to the big blue bump dilution effect. When deriving the intrinsic jet polarization P_{jet} , the presence of a very luminous disc, as assumed by the one-zone model used to interpret the observed SEDs, would imply that the correction for the thermal emission contribution becomes noticeable as the flux approaches the observed minimum level. This would lead to much higher P_{jet} values than the observed ones, and P_{jet} would not maintain the general correlation with flux shown in Figure 2.










Partly based on data taken and assembled by the WEBT Collaboration and stored in the WEBT archive at the Osservatorio Astrofisico di Torino—INAF.⁴⁰ For questions about data availability, contact the WEBT President Massimo Villata (villata@oato.inaf.it).

⁴⁰ <http://www.oato.inaf.it/blazars/webt/>

We would like to acknowledge the financial support of ASI under contract to INAF: ASI 2014-049-R.0 dedicated to SSDC. Part of this work is based on archival data, software, or online services provided by the ASI SSDC. The research at Boston University was supported by National Science Foundation grant AST-1615796 and NASA Swift Guest Investigator grant 80NSSC17K0309. This research was partially supported by the Bulgarian National Science Fund of the Ministry of Education and Science under grant DN 08-1/2016. The Skinakas Observatory is a collaborative project of the University of Crete, the Foundation for Research and Technology—Hellas, and the Max-Planck-Institut für Extraterrestrische Physik. The St. Petersburg University team acknowledges support from Russian Science Foundation grant 17-12-01029. This article is partly based on observations made with the telescope IAC80 operated by the Instituto de Astrofísica de Canarias in the Spanish Observatorio del Teide on the island of Tenerife. The IAC team acknowledges the support from the group of support astronomers and telescope operators of the Observatorio del Teide. Based (partly) on data obtained with the STELLA robotic telescopes in Tenerife, an AIP facility jointly operated by AIP and IAC. This work is partially based upon observations carried out at the Observatorio Astronómico Nacional on the Sierra San Pedro Mártir (OAN-SPM), Baja California, Mexico. C.P., V.V. and M. T. also thank Professor A. Cavaliere for the insightful discussion.

Software: AGILE software Package (AGILE SW 5.0 SourceCode), XRTDAS (v.3.1.0), XSPEC and HEASoft package (v. 6.17).

ORCID iDs

C. Pittori  <https://orcid.org/0000-0001-6661-9779>
 F. Lucarelli  <https://orcid.org/0000-0002-6311-764X>
 F. Verrecchia  <https://orcid.org/0000-0003-3455-5082>
 C. M. Raiteri  <https://orcid.org/0000-0003-1784-2784>
 V. Vittorini  <https://orcid.org/0000-0002-1208-8818>
 M. Tavani  <https://orcid.org/0000-0003-2893-1459>
 S. Puccetti  <https://orcid.org/0000-0002-2734-7835>
 S. Vercellone  <https://orcid.org/0000-0003-1163-1396>
 A. Morselli  <https://orcid.org/0000-0002-7704-9553>

References

Abdo, A. A., Ackermann, M., Ajello, M., et al. 2010, *Natur*, 463, 919
 Acero, F., Ackermann, M., Ajello, M., et al. 2015, *ApJS*, 218, 23
 Ackermann, M., Anantua, R., Asano, K., et al. 2016, *ApJL*, 824, L20

Albert, J., Aliu, E., Anderhub, H., et al. 2008, *Sci*, 320, 1752
 Bottcher, M., Basu, S., Joshi, M., et al. 2007, *ApJ*, 670, 968
 Breeveld, A. A., Landsman, W., Holland, S. T., et al. 2011, in AIP Conf. Proc., Gamma-Ray Bursts 2010, ed. J. E. McEnery, J. L. Racusin, & N. Gehrels (Melville, NY: AIP), 373
 Bulgarelli, A., Parmiggiani, N., Pittori, C., et al. 2017, *ATel*, 10563, 1
 Bulgarelli, A., Trifoglio, M., Gianotti, F., et al. 2014, *ApJ*, 781, 19
 Burrows, D. N., Hill, J. E., Nousek, J. A., et al. 2004, *Proc SPIE*, 5165, 201
 Chatterjee, R., Jorstad, S. G., Marscher, A. P., et al. 2008, *ApJ*, 689, 79
 Fitzpatrick, E. L. 1999, *PASP*, 111, 63
 Gehrels, N., Chincarini, G., Giommi, P., et al. 2004, *ApJ*, 611, 1005
 Ghisellini, G., Celotti, A., Fossati, G., Maraschi, L., & Comastri, A. 1998, *MNRAS*, 301, 451
 Giommi, P., Padovani, P., Polenta, G., et al. 2012, *MNRAS*, 420, 2899
 Giuliani, A., Chen, A., Mereghetti, S., et al. 2004, *MSAIS*, 5, 135
 Giuliani, A., D'Ammando, F., Vercellone, S., et al. 2009, *A&A*, 494, 509
 Gu, M., Cao, X., & Jiang, D. R. 2001, *MNRAS*, 327, 1111
 Hartman, R. C., Bertsch, D. L., Fichtel, C. E., et al. 1992, *ApJL*, 385, L1
 Hayashida, M., Madejski, G. M., Nalewajko, K., et al. 2012, *ApJ*, 754, 114
 Hayashida, M., Nalewajko, K., Madejski, G. M., et al. 2015, *ApJ*, 807, 79
 Hovatta, T., Valtaoja, E., Tornikoski, M., & Lähteenmäki, A. 2009, *A&A*, 498, 723
 Johnston, K. J., Fey, A. L., Zacharias, N., et al. 1995, *AJ*, 110, 880
 Kalberla, P. M. W., Burton, W. B., Hartmann, D., et al. 2005, *A&A*, 440, 775
 Kniffen, D. A., Bertsch, D. L., Fichtel, C. E., et al. 1993, *ApJ*, 411, 133
 Larionov, V. M., Jorstad, S. G., Marscher, A. P., et al. 2008, *A&A*, 492, 389
 Lucarelli, F., Pittori, C., Verrecchia, F., et al. 2015, *ATel*, 7631, 1
 Lynds, C. R., Stockton, A. N., & Livingston, W. C. 1965, *ApJ*, 142, 1667
 MacDonald, N. R., Marscher, A. P., Jorstad, S. G., & Joshi, M. 2015, *ApJ*, 804, 111
 Mignone, A., Striani, E., Tavani, M., & Ferrari, A. 2013, *MNRAS*, 436, 1102
 Moretti, A., Campana, S., Mineo, T., et al. 2005, *Proc SPIE*, 5898, 360
 Nilsson, K., Pursimo, T., Villforth, C., Lindfors, E., & Takalo, L. O. 2009, *A&A*, 505, 601
 Paggi, A., Cavaliere, A., Vittorini, V., D'Ammando, F., & Tavani, M. 2011, *ApJ*, 736, 128
 Paliya, V. S., Sahayanathan, S., & Stalin, C. S. 2015, *ApJ*, 803, 15
 Petropoulou, M., Giannios, D., & Sironi, L. 2016, *MNRAS*, 462, 3325
 Pittori, C. 2013, *NuPhS*, 239, 104
 Raiteri, C. M., Villata, M., Carnerero, M. I., et al. 2014, *MNRAS*, 442, 629
 Raiteri, C. M., Villata, M., Lanteri, L., Cavallone, M., & Sobrito, G. 1998, *A&AS*, 130, 495
 Roming, P. W. A., Kennedy, T. E., Mason, K. O., et al. 2005, *SSRv*, 120, 95
 Schlafly, E. F., & Finkbeiner, D. P. 2011, *ApJ*, 737, 103
 Schlegel, D. J., Finkbeiner, D. P., & Davis, M. 1998, *ApJ*, 500, 525
 Sikora, M., Rutkowski, M., & Begelman, M. C. 2016, *MNRAS*, 457, 1352
 Tavani, M., Barbiellini, G., Argan, A., et al. 2009, *A&A*, 502, 995
 Tavani, M., Vittorini, V., & Cavaliere, A. 2015, *ApJ*, 814, 51
 Tavecchio, F., & Ghisellini, G. 2008, *MNRAS*, 385, L98
 Urry, C. M., & Padovani, P. 1995, *PASP*, 107, 803
 Vercellone, S., Chen, A. W., Giuliani, A., et al. 2008, *ApJL*, 676, L13
 Villata, M., Raiteri, C. M., Larionov, V. M., et al. 2008, *A&A*, 481, L79
 Vittorini, V., Tavani, M., & Cavaliere, A. 2017, *ApJL*, 843, L23
 Woo, J.-H., & Urry, C. M. 2002, *ApJ*, 579, 530